Hydration of Bromide Ion in Supercritical Water: An X-ray Absorption Fine Structure and Molecular Dynamics Study

Scott L. Wallen,[||] Bruce J. Palmer,* David M. Pfund, and John L. Fulton*

Environmental and Health Sciences Division, Pacific Northwest National Laboratory,[†] Richland, Washington 99352

Matthew Newville,[‡] Yanjun Ma,[§] and Edward A. Stern

Physics Department, University of Washington, Seattle, Washington 98195

Received: April 21, 1997; In Final Form: September 3, 1997[⊗]

X-ray absorption fine structure (XAFS) measurements and molecular dynamics simulations(MD) are used to explore the extent of Br^- ion hydration in supercritical water solutions. The structure of the first hydration shell under ambient conditions is compared to that in the supercritical region spanning a temperature range from 25 to 475 °C and pressures from 1 to 650 bar. The RbBr salt concentration was varied from 0.02 to 1.5 molal. The wide range of conditions studied allowed a detailed examination of the effect of temperature, density, and concentration on the extent of ion hydration under supercritical conditions. The present results provide important new insights into factors affecting ion hydration in supercritical water. Changing the density of the supercritical solution by a factor of 1.5 causes only minor changes in the extent of ion hydration at 425 °C, whereas a pronounced dehydration occurs as the temperature is increased from 25 to 475 °C. Specifically, the number of water molecules in the first hydration shell is reduced from 7.1(±1.5) under ambient conditions to 2.8(±0.4) under the supercritical conditions of 425 °C and 413 bar. Over a concentration range of almost two orders-of-magnitude, there is little change in the extent of hydration. MD simulations of this system are used to generate XAFS spectra that are directly compared to the experimental results. Analysis of the MD-simulated XAFS spectra verified the data reduction technique used for the high temperature conditions. There is qualitative agreement between the simulation and experiment with respect to the number of nearest neighbor waters, the nearest-neighbor distances, the degree of disorder in the first shell, and the trends of these parameters with increasing temperature. It is, however, evident that refinements in the water−bromine intermolecular potentials are required to fully capture the observed behavior under supercritical conditions.

Introduction

Supercritical water (T > 375 °C and P > 220 bar) is an interesting medium for fundamental studies of solvation since the evolution of the solute−solvent structure can be observed over a wide range of densities. It is thus possible to avoid the discontinuity in the vapor−liquid density that occurs under ambient conditions. Supercritical water also has interesting applications in the area of hazardous waste destruction.[1−5] It is also of interest from a geochemical point of view. A lot of what we know about the molecular structure in supercritical water comes from simulations.[6−8] More experimental results on the properties of supercritical water[9−11] are appearing, although there is a distinct lack of information concerning the solvation of ions in high-temperature aqueous systems. The degree of hydration of an ion in a supercritical environment is an important factor affecting solubility, reactivity, transport properties and corrosion.

In a previous study we reported the first observation of a significant reduction in the hydration number around Sr^{2+} under supercritical conditions.[12,13] In a subsequent work[14] a similar trend was observed for a monovalent cation, Rb^+. In addition, a contraction in the water−ion distance was observed in supercritical water.[14] Recently, Yamaguchi et al.[15] used neutron diffraction methods to study the hydration of Cl^- under supercritical conditions. A reduction in the waters of hydration from 5.8 to 2.5 upon increasing the temperature from ambient to 375 °C was reported, thus substantiating the earlier X-ray absorption fine structure (XAFS) results. In a related XAFS study, Seward et al.[16] recently reported the hydration of Ag^+ and Sr^{2+} ions in liquid solutions up to 350 °C at their respective vapor pressures. For Ag^+ ion, they found a similar reduction in hydration (from 4 to 3) and a contraction of the first-shell distances of approximately 0.1 Å. More recently, a neutron-scattering study[17] of the thermal effect of Cl^- hydration showed a reduction in the hydration number from 6.4 under ambient conditions to about 4.9 at 300 °C. Thus, a consistent picture is emerging from two fundamentally different techniques of a significant reduction in the waters of hydration for both cations and anions under hydrothermal conditions. At this point, it is not clear whether this reduction is due to (i) a thermal effect of breaking ion−water "bonds" at high temperature, (ii) a density effect, (iii) a result of dehydration occurring upon the formation of ion pairs, or (iv) some combination of these effects.

In this paper we use XAFS to explore the hydration of Br^- under supercritical conditions. For ion hydration, a precise measurement of the short-range structure of the first couple of solvation shells is essential for prediction of a range of ion properties in solution. In general, XAFS[18−21] is a decidedly

* Corresponding authors.
[†] Operated by Battelle Memorial Institute.
[||] Current address: Department of Chemistry, CB 3290, University of North Carolina, Chapel Hill, NC 27599.
[‡] Current address: GSECARS Building 434A, Argonne National Laboratory, 9700 Cass Avenue, Argonne, IL 60439.
[§] Sharp Microelectronics Technology, 5700 NW Pacific Rim Blvd., Camas, WA 98607.
[⊗] Abstract published in *Advance ACS Abstracts,* November 15, 1997.

S1089-5639(97)01361-3 CCC: $14.00

short-range technique in comparison to X-ray and neutron scattering where it may be possible to obtain a complete radial distribution function. There are many advantages to using XAFS for supercritical fluid studies because it isolates the pair distribution function about the atom of interest. The first-neighbor environment can be obtained with high spatial resolution. Further, XAFS measurements can be made under conditions of "infinite dilution"—very low concentrations where ion−ion interactions are negligible, thus providing the simplest experimental condition for determination of water−ion interactions. Another advantage of XAFS is that the height of the absorption edge provides a direct measure of the fluid density under any experimental condition.[14] Problems that arise due to the high compressibility of the solvent near the critical point and the necessity of high solute concentrations complicate the use of neutron and X-ray diffraction techniques (especially those based upon isotopic substitution) but are absent from the XAFS experiment. Finally, there is the possibility of deriving information on ion charge state and ion−water charge transfer from information contained in the X-ray absorption near-edge structure (XANES). In the end, it may well require accordant measurements from several techniques to confirm the structure under these conditions.

Comprehensive neutron-scattering studies, using difference methods with isotopic substitution, have been very successful at deriving the hydration structure of anions and cations under ambient conditions.[22−25] These studies have completely resolved the geometry of the water in the first shell. For cations, the oxygens of the water molecules are directly bound to the cation. For anionic species, specifically Cl^-, a proton of the water sits between the ion and the oxygen. The H−O axis of water is radially aligned to the anion. In a related molecular dynamics study of an aqueous $SrCl_2$ solution under ambient conditions, Dang et al.[26] showed a dehydration of the Cl^- as the room-temperature contact ion pair is formed.

Since supercritical fluids allow one to explore solution properties at low densities, it is useful to briefly review what is currently known about structure in the extreme of low-density−gas phase clusters. From mass spectrometric studies of small ion-water clusters we know that as more waters are added to the first solvation shell they are less strongly bound. There is an incremental decrease in the hydration enthalpy, $\Delta H_{n-1,n}$ with each consecutive water molecule.[27,28] For the Br^-, the enthalpy change going from 5 to 6 water molecules is about $\Delta H_{5,6} =$ 10.5 kcal/mol, in comparison to $\Delta H_{0,1} = 12.6$ kcal/mol for the first water molecule that is more tightly bound. Results for Cl^- are just 4 % higher over this range pointing to the chemical similarity of Br^- and Cl^-. Corresponding values for the Rb^+ counterion are $\Delta H_{5,6} = 10$ kcal/mol and $\Delta H_{0,1} = 16$ kcal/mol. An interesting observation from ab initio calculations of small ion−water clusters is that cations are typically embedded in a shell of water molecules. For anions, however, many of the optimized geometries for small clusters shows the anion sitting on the surface of the small water cluster.[29,30] It is these nuances that may be important factors affecting structure and reactivity under supercritical conditions where the extent of hydration is greatly reduced. Eventually, the elucidation of the detailed hydration structure will inevitably evolve from X-ray- and neutron-based studies.

Whereas in our earlier papers we have used XAFS to explore the hydration of monovalent and divalent cations under supercritical conditions, in the present study, we examine bromide as the monovalent anion. This represents the most extensive examination of supercritical ion hydration, exploring in detail, the effects of fluid density and temperature and the ion concentration. It is worthwhile to mention that there have been several XAFS studies of aqueous Br^- hydration under ambient conditions.[31−35] Generally these studies agree with coordination number and distance of 6 and 3.2−3.4 Å, respectively, that have been determined using diffraction techniques.[36]

XAFS Experimental Methods

Experimental techniques have been described in detail elsewhere and are only briefly summarized here.[12,14] The high-temperature, high-pressure XAFS cell was fitted with two opposing 3 mm diameter × 0.5 mm thick synthetic diamonds that were produced by chemical-vapor-deposition providing a polycrystalline structure to minimize interference with the XAFS spectroscopy. These X-ray windows were mounted in such a way as to provide a 5.8 mm path length. The body of the cell was constructed from a high-nickel alloy and then internally plated to a thickness of 50 μm with platinum. The temperature of the cell was maintained to within ±1 °C using a three-mode controller (Omega, No. CN3000), whereas the fluid pressure was measured to within ±1 bar using an electronic transducer (Precise Sensors, Inc., No. D451) which was calibrated against a deadweight tester (Ashcroft, No. 1305-D).

Bromine K-edge XAFS spectra were collected on beamline X-19A of the National Synchrotron Light Source (NSLS) at Brookhaven National Laboratory. Two focusing mirrors were used to produce a beam diameter of approximately 1-2 mm that was aligned such that the beam passed cleanly through the cell. The beamline used a Si(2,2,0) double crystal monochromator which was detuned 60% to reduce the content of the higher harmonics. The spectrum reported for liquid and supercritical water solutions consisted of five summed spectra that were acquired over a total time of approximately 3 h. A background spectrum of pure water under identical conditions was subtracted from each of the sample spectra. All spectra except the 0.02 molal solutions were acquired using a standard transmission detector arrangement. For increased sensitivity with the 0.02 m solutions, a 13-element liquid-N_2-cooled Ge detector was used to collect the XAFS data in fluorescence mode. This detector was tuned to reject elastic scattering of the incident beam by creating a gated energy window that accepted about 90% of the Br fluorescence. The fluorescence detector was placed downstream of the cell and was aligned so that it would collect the cone of fluorescence emission from about 0.3 to 10° while excluding the incident beam with a beam stop.

Typically, experiments were started at the highest pressure and subsequent spectra were collected at lower pressures by discharging small amounts of the solution through a valve. The discharged solution traveled through a short section of tubing which was immersed in a water bath to act as a condenser. The condensate from this line could then be discharged directly to the pan of an electronic balance (Mettler Toledo AG204) in order to determine the density of the supercritical fluid solution under any condition based upon the known volume of the cell.[14]

XAFS Spectra Analysis

The methods for data collection, background correction and data transformation are well-established.[21,37,38] The XAFS oscillations, $\chi(k)$, were extracted from the experimentally measured absorption coefficient $\mu(E)$ by subtracting an isolated "embedded" atom background function, $\mu_0(E)$, according to the relationship $\chi(k) = (\mu(E) - \mu_0(E))/\Delta\mu_0(E_0)$. Here, the wavenumber of the ejected photoelectron is given by $k = (2m_e(E - E_0)/\hbar^2)^{1/2}$ where E_0 is the absorption edge energy for the K-edge of the absorbing atom and $\Delta\mu_0(E_0)$ is the edge-jump normaliza-

tion constant. We used an automated background subtraction method (AUTOBAK) developed by Newville et al.[39] for removal of $\mu_0(E)$. This method systematizes the k-space placement of the cubic spline function that is used to approximate the postedge absorbance from an isolated atom. The placement of the spline is chosen as to minimize the R-space features at distances that are well below the atom−atom contact distance. For the Br^- system, this minimum R-space distance, R_{bkg}, was chosen as 1.4 Å. The number of equally spaced knots of the cubic spline in k-space is simply equal to $(1 + 2\Delta k R_{bkg}/\pi)$ as prescribed by information theory. For Br, there are weak 1s4s, 1s3d, and 1s3p multielectron excitations[40−43] at $k = 3.0$, 5.0, and 7.5 $Å^{-1}$. These were removed from the XAFS spectra by direct subtraction of a properly scaled multielectron spectrum of HBr (Figure 3 of ref 42). This procedure removed the multielectron contribution to $\mu_0(E)$.

The analysis of the $\chi(k)$ function was based upon the standard XAFS relationship

$$\chi(k) = \frac{F(k)S_0^2N}{kR^2} e^{-2k^2\sigma^2} e^{-2R/\lambda(k)} \sin\left(2kR + \delta(k) - \frac{4}{3}k^3C_3\right) \quad (1)$$

where $F(k)$ is the backscattering amplitude of a particular shell, S_0^2 is the constant factor describing the relaxation of the passive electrons in the presence of a core hole, $\delta(k)$ is the photoelectron phase shift and $\lambda(k)$ the mean-free path of the photoelectron. $F(k)$, $\delta(k)$, and $\lambda(k)$ are derived from the theoretical standard FEFF[44], whereas we use the value of $S_0^2 = 0.91$ for Br that has been previously measured by Frenkel et al.[40] The remaining terms in eq 1 that describe the water−ion structure include N, the coordination number of the near-neighbor shell, R, the near-neighbor distance, σ^2, the mean-square variation in R due to both static and thermal disorder, and finally C_3, the anharmonicity of the pair distribution, also known as the third cumulant. These terms, that contain the quantitative structural information, were found using the FEFFIT[45,46] analysis program that employs a nonlinear, least-squares fit to the theoretical standards calculated by FEFF.[44] In addition to the structural parameters, a single nonstructural parameter, ΔE_0, is varied to account for the simple estimate of this energy made by FEFF. A refined ΔE_0 value of 5.60 eV above the first K-edge inflection point was used. The FEFF calculations for Br−O were done with atomic configurations based upon the crystallographic structure of $NaBrO_3$.[47] The $\chi(k)$ data were weighted by k^2, windowed between $1.8 < k < 6.0-7.8$ $Å^{-1}$ using a Hanning window with $dk = 1.0$. For the ambient spectra, the k range of the fit was from 2.75 to 7.8 $Å^{-1}$. The fitted parameters did not vary even as the minimum k was increased to 4.0 $Å^{-1}$. For minimum k values below 2.75 $Å^{-1}$, the amplitudes from FEFF were too small in addition to some small errors in the phase shift leading to unrealistic fitting results. There are two possible sources of this error, one arising from the reduced reliability of the FEFF calculation in this low k region and the other arising from the focusing effect of those hydrogen atoms on the water that reside between the oxygen and the Br^- ion that are known to increase the scattering amplitudes in the low k region.[48] Thus, using the ambient data, the amplitude and phase shift of the theoretical standard was revised in the k region from 1.5 to 2.75 $Å^{-1}$ to adequately fit the data. This modified theoretical standard was then used for all conditions at elevated temperature. The fit range for the high-temperature data was from $1.8 < k < 6.0$ $Å^{-1}$ excepting the 1.5 m solutions that were fit from $1.8 < k < 7.8$ $Å^{-1}$ because of the low noise of the high k region for this data. All the fits were done on both the real and imaginary parts of $\tilde{\chi}(R)$ in the region of $1.6 < R < 4.0$ Å. The uncertainties reported in Table 3 and 4 increase the misfit between the data and the best fit model by an amount of $1/\nu$, where ν is the degrees of freedom in the fit (typically, $\nu = 2$ for the Br^- data). Analysis of the reduced χ-squared statistic from the fits indicates that the errors are dominated by the systematic errors of the theory or the fitting routine rather than by the random fluctuations of the data.

TABLE 1: Pair-Potential Parameters for the MD Simulations

atom	σ (Å)	ϵ (kcal/mol)	q (|e|)	α (Å^3)
O	3.196	0.160	−0.730	0.528
H	0.000	0.000	0.365	0.170
Rb	3.671	0.0845	1.000	1.40
Br	4.686	0.100	−1.000	4.77

Molecular Dynamics Simulation

Molecular dynamics simulations were used to obtain simulated XAFS spectra that could be used in analyzing the experimental spectra. Simulations of the RbBr system at 298 and 697 K were performed using a polarizable model for the intermolecular interactions. This model consists of pairwise interactions between all atomic sites of the form

$$\phi_{ij}(r_{ij}) = 4\epsilon_{ij}\left[\left(\frac{\sigma_{ij}}{r_{ij}}\right)^{12} - \left(\frac{\sigma_{ij}}{r_{ij}}\right)^{6}\right] + U_C \quad (2)$$

$$U_C = \sum_{i<j}\frac{q_iq_j}{r_{ij}} - {}^1/_2\sum_i \mathbf{p}_i\cdot\mathbf{E}_i \quad (3)$$

The parameters σ_i, ϵ_i, and q_i were defined for each atomic species i, the parameters appearing in eq 2 were then obtained using the combining rules $\epsilon_{ij} = (\epsilon_i\epsilon_j)^{1/2}$ and $\sigma_{ij} = (\sigma_i + \sigma_j)/2$.

The remaining parameters (apart from q_i) defining the Coulomb interactions in eq 3 are the induced dipole $\mathbf{p}_i$ at site i and the local electric field, $\mathbf{E}_i$, due to all the other fixed charges in the system. The induced dipole $\mathbf{p}_i$ is given by the expression

$$\mathbf{p}_i = \alpha_i(\mathbf{E}_i + \sum_{i\neq j}\mathbf{T}_{ij}\cdot\mathbf{p}_j) \quad (4)$$

where α_i is the polarizability associated with site i and $\mathbf{T}_{ij}$ is the dipole tensor used to described the electric field due to a dipole

$$\mathbf{T}_{ij} = \frac{1}{r_{ij}^3}\left(3\frac{\mathbf{r}_{ij}\mathbf{r}_{ij}}{r_{ij}^2} - 1\right) \quad (5)$$

The dipole moments on each atomic site were calculated using an iterative procedure. Because this requires several repetitions of the force calculation at each time step, this model uses significantly more computer time than a conventional molecular dynamics simulation using a non-polarizable force field. To reduce the computer time needed to run simulations with this model, a molecule-based cutoff was used, where the interactions between pairs of molecules are set equal to zero whenever the centers of mass of the two molecules are separated by more than 8.5 Å. The POL1 parameters for water[49] were used in these simulations, the parameters for Rb^+ were adapted from ab initio calculations on the rubidium-water dimer,[50] and the parameters for Br^- were taken from a nonpolarizable model[51] and augmented by the atomic polarizability of the bromide ion. All parameters used in these calculations are summarized in

TABLE 2: Comparison of Bromide Ion−Water Distances and Water Coordination Numbers Measured by XAFS for Solutions under Ambient Conditions

[Br^-], M	N	R, Å	σ^2, Å^2	C_3
0.150[a]	6.9	3.34	0.04	0.00648
0.10[b]		3.19	0.028	
1.0[c]	5.3	3.26	0.023	
4.6[d]		3.30	0.031	
0.2[e]	7.1(1.5)	3.35(07)	0.025(06)	−0.0018(27)
1.5[e]	7.2(0.4)	3.36(01)	0.027(02)	−0.0014(06)

[a] Reference 31. [b] References 32 and 33 assumes $N = 6$. [c] Reference 34, weighted average distance. [d] Reference 35. [e] This work, concentrations in molality.

Table 1. The POL1 model used a water geometry with an OH bond distance of 1.0 Å and an HOH bond angle of 109.47 degrees.

The oxygen−ion radial distribution functions were integrated over the distance r to get the number of nearest-neighbor water molecules as a function of distance, $N(R)$, using the formula,

$$N(R) = 4\pi\rho\int_0^R G(r)r^2\,dr \qquad (6)$$

where ρ is the average density of water atoms in the system.

All simulations consisted of 235 rigid water molecules plus two Rb^+ and two Br^- ions, corresponding to a 0.473 m solution of RbBr. The system sizes were adjusted so that the density of the 298 K simulation was 1.066 g/cm^3 and the density of the 697 K simulation was 0.640 g/cm^3. Velocity scaling was used to control the temperature. A time step of 2 fs was used for the simulations at 697 K. The polarizable model was found to be less stable at lower temperatures and thus, a shorter time step of 1 fs was used for the simulations at 298 K. Each simulation was run for 50 ps.

Every 0.2 ps, a configuration was saved to a file, resulting in a total of 250 configurations for each simulation. Two clusters were extracted from each configuration, one for each bromine atom. Each cluster contained a Br^- ion at the center, plus all other atoms, except hydrogen, falling within 5 Å of the central Br^- ion. These clusters were used as input for a calculation of the bromine XAFS spectrum using the FEFF6 multiple-scattering code. The hydrogen atoms were left out of the calculation because they were found to significantly distort the results of the FEFF calculation.[13] The 500 individual bromine spectra were then averaged together to obtain a solvent averaged bromine XAFS spectrum that can then be compared directly to experiment. This calculation is similar to one described previously for $SrCl_2$ solutions.[13]

Results

Figure 1 shows the XAFS spectra acquired over temperatures ranging from ambient to supercritical under constant pressure conditions. Figure 2 shows the effect of density under a constant supercritical temperature. As has been previously described,[14] the height of the absorption edge is a convenient and accurate method of measuring the density of the supercritical fluid solution. Since these experiments are conducted at constant molality and at a fixed path length, the amount of Br^- in the beam is directly proportional to the fluid density. Such a direct density measurement is an essential parameter for interpretation of results and for relating these results to theory or simulation. Indeed, addition of the RbBr salt substantially increases the critical temperature of the solution above that of pure water; thus, the solution densities are much higher than for pure water at the same temperatures and pressures. Values of density

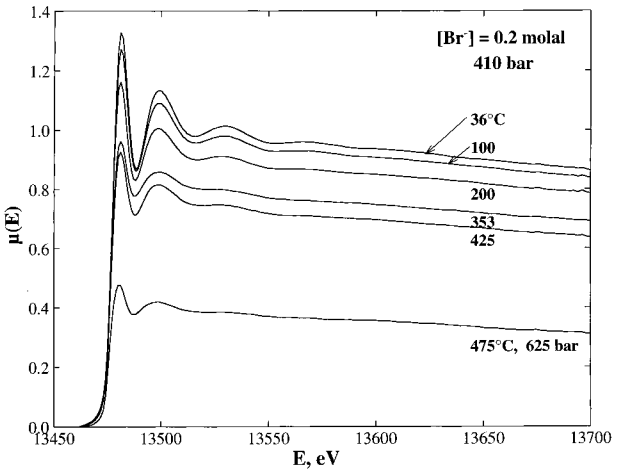

Figure 1. XAFS spectra for a series of temperatures from 36° to 475 °C. The concentration of Br^- ion is 0.2 m in all cases, and the pressure is 410 bar, except the 475 °C data where the pressure is 625 bar.

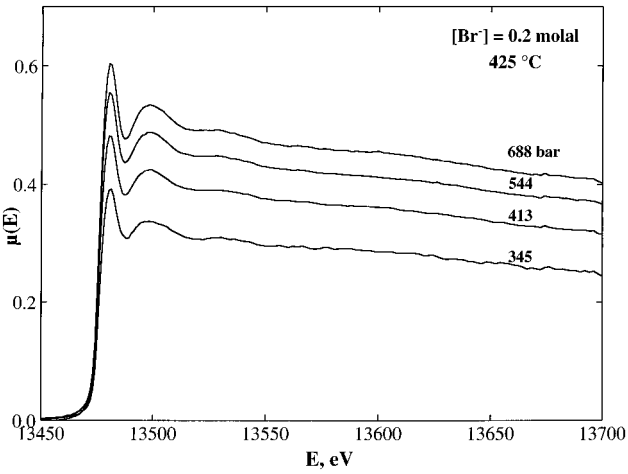

Figure 2. XAFS spectra for a series of pressure from 345 to 688 bar. In all cases the concentration of Br^- ion is 0.2 molal and the temperature is 425 °C.

determined by this method are given in Table 3. In Figures 1 and 2, the edge height is substantially reduced under all supercritical conditions and especially those conditions having low density. In addition, the amplitude of the XAFS oscillations on the high-energy side of the edge decreases in a fashion that is disproportionate to the edge height for the temperature series but remains approximately proportional to the edge height for the pressure series. The phase behavior of the system was found to be very similar to that of the NaCl−H_2O system.[52] For the conditions that we have explored, the nature of the phases, e.g., liquid−vapor equilibria, and the positions of the phase boundary were very similar to that of monovalent salt, NaCl. Only the single-phase region was explored for all conditions of this study.

Figures 3−5 give the k^2-weighted $\chi(k)$ plot for the temperature, density, and concentration series. As shown in Figure 3, increasing the temperature from ambient to the supercritical region produces a dramatic change in the hydration structure. Several qualitative observations can be made directly from this plot. First, the decrease in the amplitude of the oscillations is primarily due to a decrease in the hydration number of the first water solvation shell (See eq 1.). A second important attribute of the spectra in Figure 3 is that the amplitude of the oscillations are damped at higher k, but there is little change in the extent of damping when comparing the different temperature series. Thus, no large changes in σ^2 occur as the temperature is increased (see eq 1).

TABLE 3: Results[a] of XAFS Analysis of Br^- Hydration under Liquid and Supercritical Conditions

[Br^-], m^a	T, °C	P, bar	ρ, g/cm^3	N	R, Å	σ^2, Å^2	$C_3 \times 10^3$	R^b
0.2	36	412	1.04	7.1(1.5)	3.35(07)	0.025(06)	−1.8(2.8)	0.012
0.2	100	412	1.01	6.7(0.5)	3.36(01)	0.028(03)	−0.7(0.7)	0.003
0.2	200	419	0.953	5.2(0.6)	3.38(01)	0.028(04)	1.7(1.2)	0.008
0.2	353	421	0.783	4.7(1.1)	3.37(03)	0.037(08)	1.9(2.8)	0.013
0.2	425	345	0.327	3.0(0.5)	3.35(07)	0.025[c]	0.0(8.0)	0.061
0.2	425	413	0.419	2.8(0.4)	3.41(02)	0.023(07)	5.4(2.0)	0.010
0.2	425	544	0.484	2.8(0.9)	3.39(04)	0.021(13)	3.4(4.3)	0.021
0.2	425	688	0.514	2.9 (0.9)	3.38(04)	0.024(12)	2.5(4.2)	0.018
0.2	475	625	0.833	3.1(0.6)	3.40(03)	0.031(09)	6.3(3.0)	0.006
0.02	29	1		6.9(1.5)	3.40(03)	0.023(09)	2.0(3.0)	0.009
0.02	200	412		5.4(1.1)	3.36(03)	0.033(09)	0.0(3.0)	0.007
0.02	427	412		2.7(0.6)	3.39(03)	0.024(10)	4.9(3.4)	0.011
1.5	26	1		7.2(0.5)	3.36(01)	0.027(02)	−1.4(0.6)	0.002
1.5	425	414		2.1(0.4)	3.36(02)	0.023(05)	2.2(1.5)	0.020
1.5	425	500		2.0(0.3)	3.37(02)	0.024(04)	1.8(1.2)	0.011

[a] Concentration in molality. [b] Goodness of fit defined by a scaled sum of squares as described in FEFFIT.[45,46] [c] Fixed in the fitting since this spectrum has higher noise.

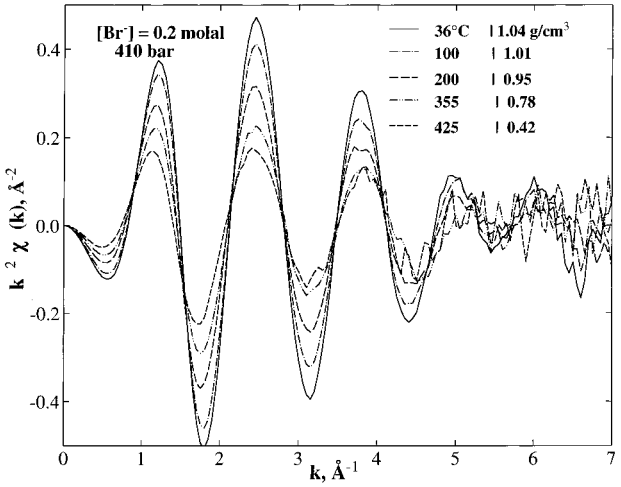

Figure 3. k^2-weighted $\chi(k)$ plots for the temperature series at constant pressure (410 bar) given in Figure 1.

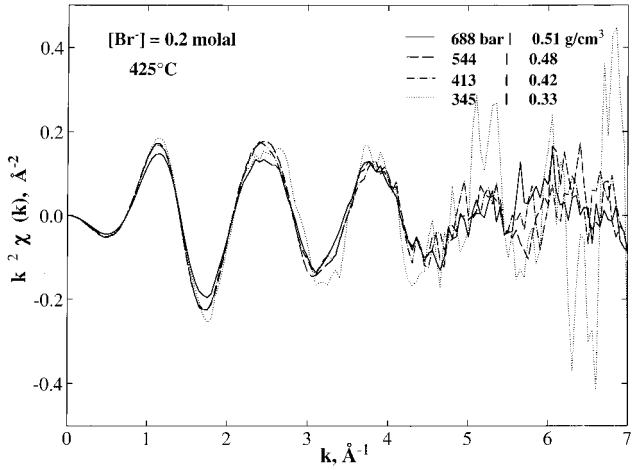

Figure 4. k^2-weighted $\chi(k)$ plots for the pressure series at constant temperature (425 °C) given in Figure 2.

Figure 4 shows the effect of changing the fluid density at a supercritical temperature of 425 °C and a Br^- concentration of 0.2 m. The lowest density studied at 425 °C is just above the phase boundary for the vapor−liquid equilibrium. Although the density changes by almost a factor of two, the hydration shell remains unchanged since the XAFS amplitudes and phases remain essentially constant over this wide range of densities. This observation is in qualitative agreement with MD simulations of chloride ion in supercritical water.[53,54] For the density range in this study, a no change in hydration was observed but one can anticipate that as the density is reduced well below 0.1 g/ml, that some dehydration would occur. Finally, in Figure 5 we see the effect of changing the concentration by almost two orders-of-magnitude on the local hydration structure. For this series, the temperature is 425 °C at a pressure of 415 bar. For a change in concentration from 0.02 to 0.2 m, there are very minor changes in the XAFS spectra, and we can conclude that the hydration structure is mostly unaffected by salt concentration over this range. At 1.5 m there is a modest decrease in the amplitudes in the lower k region which is perhaps related to further dehydration of the ion upon formation of multiple ion-pair associations.

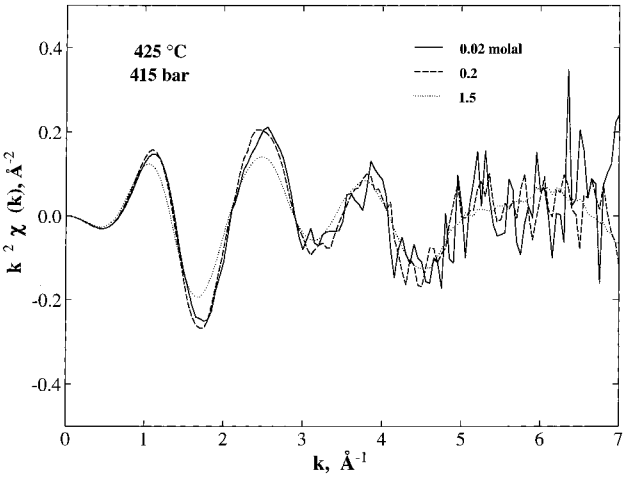

Figure 5. k^2-weighted $\chi(k)$ plots for three different Br^- concentrations at 425 °C and 415 bar.

Discussion

Experimental XAFS Data. Table 2 gives a comparison of the measured Br^- ion-to-O distances and coordination numbers determined in the present study under ambient conditions to the values reported by others. The distances and coordination numbers determined in this study are in general agreement with previously reported values from other XAFS investigations.[31−35] The values are also in good agreement with the coordination numbers and distances (6 and 3.2−3.4 Å, respectively) that are derived from diffraction-based studies.[36] The measured coordination number is also consistent with neutron scattering results for Cl^- at room temperature in which a value of 6.4 was reported.[17]

Table 3 gives a complete list of fitted results for the various sub-critical and supercritical conditions. Typical examples of

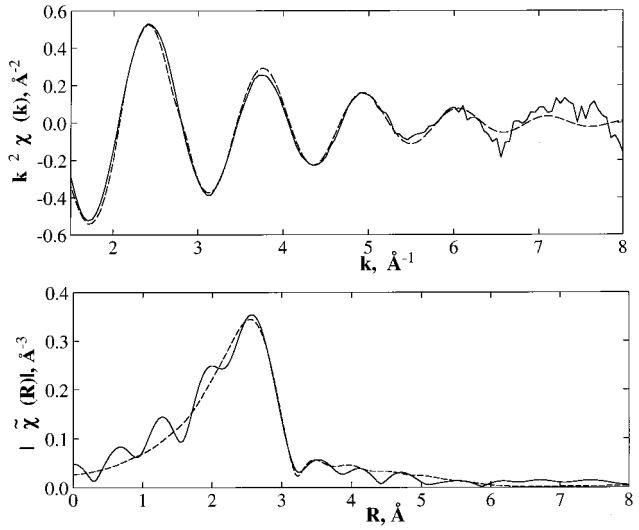

Figure 6. An XAFS k^2-weighted $\chi(k)$ plot and $|\tilde{\chi}(R)|$ plot for 0.2 m Br^- in ambient water. The solid line shows the experimental data and the dashed line shows the best-fit model using FEFF calculations and the parameters listed in Table 3.

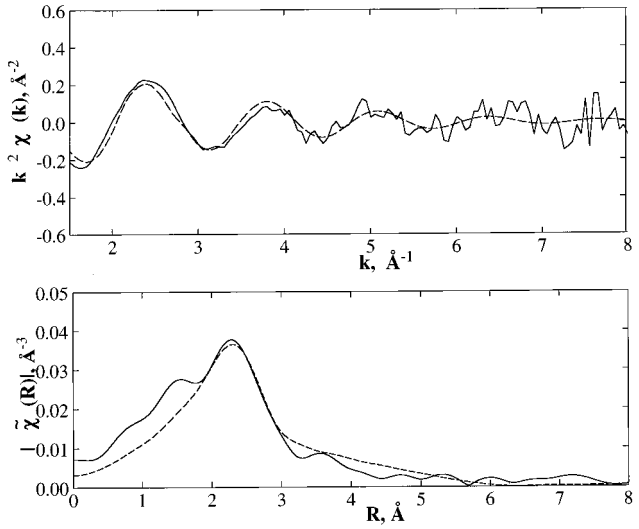

Figure 7. An XAFS k^2-weighted $\chi(k)$ plot and $|\tilde{\chi}(R)|$ plot for 0.2 m Br^- in water at $T = 425$ °C and $P = 413$ bar. The solid line shows the experimental data and the dashed line shows the best-fit model using FEFF calculations and the parameters listed in Table 3.

the quality of the fits are given in Figures 6 and 7 showing experimental and model fits in both *k* and *R* space for an ambient and a supercritical condition, respectively. The effect of temperature on the measured coordination numbers and nearest-neighbor distances is consistent amongst the three different concentrations studied—0.02, 0.2, and 1.5 *m*. The first coordination shell experiences approximately a 61% dehydration from 7.1 neighboring water molecules under ambient conditions to 2.8 neighbors under supercritical conditions at 425 °C. This observation is similar to our previous results for monovalent and divalent cations under supercritical conditions.[12−14] The distance of the nearest neighbors remains almost unchanged although there is a trend toward slightly increasing distances at high temperature. Changing the density by a factor of about 1.5, from 0.33 to 0.51 g/cm^3, does not alter the coordination number or nearest neighbor distances significantly. The effect of density and temperature on the extent of hydration of anions is in qualitative agreement with recent MD simulations for Cl^- ion by Chialvo et al.[53]

Figure 8 presents a plot of the coordination number, *N*, as a function of temperature that includes all three concentrations

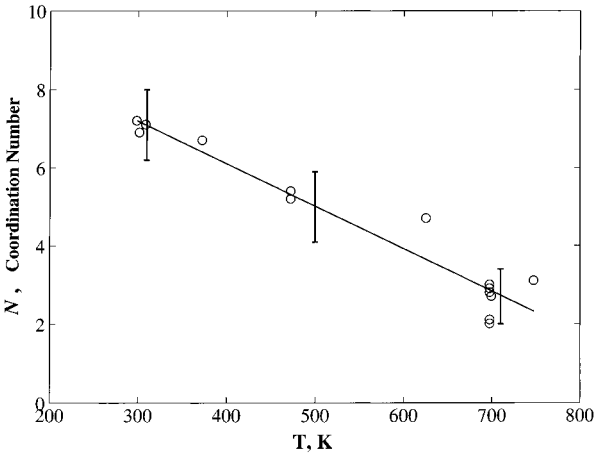

Figure 8. Water coordination number in the first shell around the Br^- ion plotted versus the temperature of the system. The plot includes all the conditions of concentration and pressure given in Table 3. The line is the least squares fit to the data points.

and all pressures. The simple linear relationship with temperature is similar to that observed for the change in the extent of intermolecular hydrogen bonding of pure water given by Gorbaty et al.[9]

It is useful to compare the measured extent of dehydration for Br^- with recently reported values for the chemically similar Cl^- made by neutron diffraction. Yamaguchi et al.[15] reported a 57% reduction in hydration (as measured by nearest-neighbor ^2H) upon increasing the temperature from 25 to 375 °C. This is in reasonable agreement with the present results where a 34% reduction was observed from 36 to 353 °C. The trend of significant dehydration at elevated temperature is also consistent with another recent neutron scattering study[17] reporting a 23% reduction in the hydration (6.4 to 4.9) of Cl^- upon increasing the temperature from 25 to 300 °C.

Table 3 gives the measured σ^2 for all conditions. As the temperature is increased from ambient conditions to 353 °C, σ^2 increases in accord with the higher thermal disorder of the system. Under supercritical conditions all of the measured σ^2 values are closer to their values under ambient conditions. Under supercritical conditions there is more uncertainty in the measured σ^2 and thus we cannot say with high confidence that σ^2 is decreased. However for the 1.5 m solutions, where the data are of sufficient quality to get a better measure of the σ^2, the smaller value appears to be statistically significant. We know from gas-phase cluster studies that the binding energies of the first few water molecules are substantially higher than those of the fully saturated first shell. Thus a smaller σ^2 might be anticipated. In addition, as will be discussed in a following section, the measurement of the nearest neighbor waters may also include contributions from the Rb^+ counter ion. Thus the much higher mass of this atom would also reduce σ^2 if the binding energy were about the same as for a water molecule. There is also a possibility that there may be bridging waters between the ion pairs that have much lower σ^2 than for water molecules that only bind to the anion. We will address this aspect in a future paper dealing with MD results of similar systems.

As the temperature of the system increases, the anharmonicity parameter, C_3, increases. If the C_3 term is left out of the fits, an apparent contraction of the nearest-neighbor water distance of about 0.1 Å is observed, whereas inclusion of C_3 leads to a slight increase in the distances of the nearest-neighbor waters. Thus C_3 is a significant and important parameter to account for the anharmonicity of the system. It should be strongly

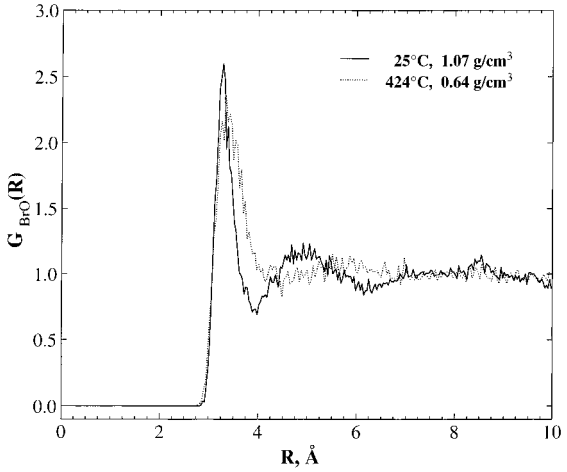

Figure 9. Radial pair distribution function from molecular dynamics simulation for the bromide−oxygen distance under ambient (T = 25 °C) and supercritical (T = 424 °C) conditions. Derived from the same 250 configurations that were use to generate the XAFS spectra in Figure 11.

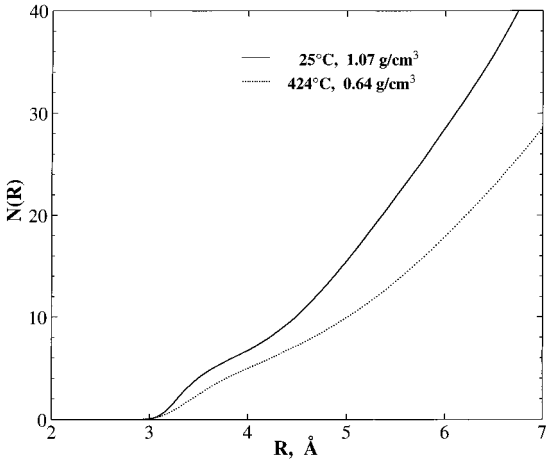

Figure 10. Number of water molecules around the bromide ion as a function of distance for the ambient (T = 25 °C) and supercritical (T = 424 °C) conditions. These were obtained by integration of the G_{BrO}-(R) plots given in Figure 9.

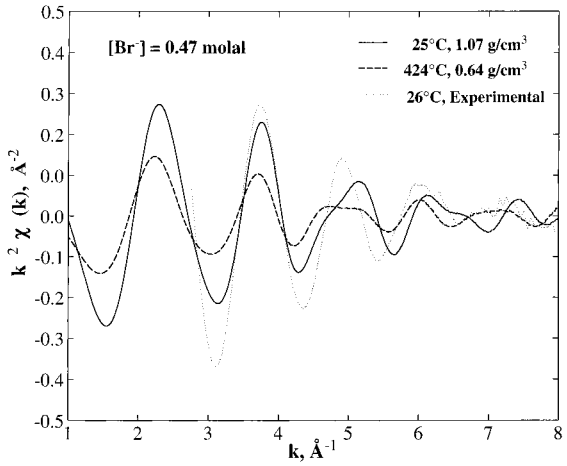

Figure 11. Plot of $k^2\chi(k)$ generated from the MD simulation for the ambient (T = 25 °C) and supercritical (T = 424 °C) conditions. For comparison, the experimentally derived $k^2\chi(k)$ spectra at 36 °C is also shown.

emphasized that, even with the uncertainties associated with the measurement of σ^2 and C_3, the substantial reduction in the extent of hydration remains a statistically significant result of the data as demonstrated by the global analysis of the errors presented in Table 3.

The change in the number of nearest neighbors is consistent with a reduction in the number of ion-water bonds at the high temperature of the system. This reduction may also be in part due to the formation of an appreciable concentration of contact ion pairs. The present simulation results and those of Chialvo et al.[6] show that an extensive amount of ion pairing exists under supercritical conditions even at concentrations as low as 1×10^{-3} M. A recent MD simulation study of liquid phase solutions[26] indicates that, upon formation of the ion pair, an appreciable degree of dehydration occurs for a divalent cation. A similar phenomena is expected under supercritical conditions. Thus both thermal dehydration and ion-pair dehydration may contribute to the measured changes in the number of nearest-neighbor waters.

MD Simulated XAFS. The $G_{BrO}(R)$ given in Figure 9 gives possible clues to the water structure in the first and second shells and changes in the shell structure under supercritical conditions. The position of the first peak in $G_{BrO}(R)$ increases from 3.30 to 3.43 Å representing an expansion of the first water shell at elevated temperature. This is perhaps slightly larger than the experimental results shown in Table 3. The first peak also broadens substantially at high temperature. A first approximation fit to this peak with a Gaussian function yields an increase in σ^2 from 0.043 to 0.135. Further, the order in the second water shell located at 4.9 Å is largely destroyed under supercritical conditions. The number of water molecules in the first hydration shell diminishes as shown in the integrated G_{BrO}-(R) plot shown in Figure 10. This represents a reduction from 5.0 (3.64 Å shell) at 25 °C to 4.5 (3.94 Å shell) at 424 °C. This corresponds to a 10% reduction which is substantially less than the 61% reduction measured experimentally over the same temperature range.

Multiple configurations downloaded from the MD simulations were used to generate the configurationally averaged XAFS spectra given in Figure 11. A powerful way of validating the data reduction technique (FEFFIT) is to apply the same analysis to both the simulated spectra and the experimental data. This approach allows one to clarify the effects of disorder on the derived parameters and also provides a stringent test of the validity of the water-ion potentials used in the simulations. The results of the FEFFIT analysis for the simulated spectra are given in Table 4. Under ambient conditions there is good agreement between N, R, and σ^2 derived from FEFFIT of the simulated spectra and the corresponding values reported above from the $G_{BrO}(R)$ in Figure 9. Under supercritical conditions, N and σ^2 derived from FEFFIT of the simulated spectra are underestimating the values from $G_{BrO}(R)$. This may be in part due to the limited number of configurations used in the generation of XAFS spectra resulting in lower quality data at higher k. It may also point to a need to be careful in interpreting the parameters derived from the fits to the high-temperature XAFS spectra. The agreement with the experimentally derived N values is also not good and this most likely points to the limited range of application of the water−ion intermolecular potentials used in the simulation. Clearly, the intermolecular potential needs to be revised to capture the features of the high-temperature structure.

Several of the MD configurations were analyzed using FEFF to explore the importance of multiple scattering paths (>three atom paths) for the Br^-−water system. The contribution from multiple scattering to calculated $\chi(k)$ was found to be less than 3%. This is below the noise level of the experimental data and is thus not considered in the analysis. This is the same

TABLE 4: Parameters Extracted from the MD-Simulated XAFS Using the Same Data Reduction Procedure as Applied to the Experimental Data in Table 3

[Br^-], *m*	*T*, °C	ρ, g/cm^3	*N*	*R*, Å	σ^2, Å^2	$C_3 \times 10^3$	*R*[a]
0.47	25	1.07	4.6(0.5)	3.31(02)	0.026(04)	2.8(1.2)	0.009
0.47	424	0.64	2.7(0.5)	3.35(03)	0.034(08)	1.1(2.7)	0.028

[a] Goodness of fit defined by a scaled sum of squares as described in FEFFIT.[45,46]

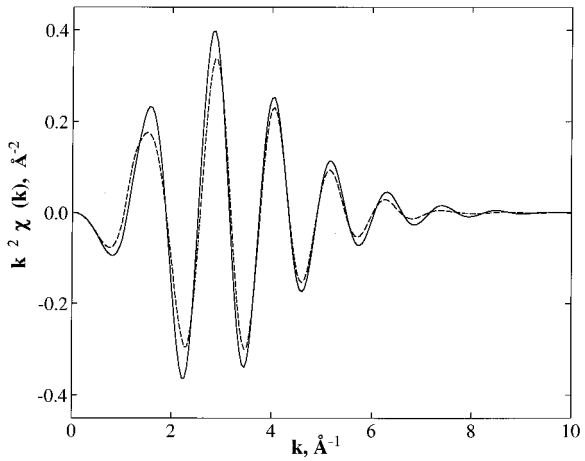

Figure 12. FEFF-generated $k^2\chi(k)$ plot for Br^- with and without the cation contact-ion pair. The solid line represents octahedrally coordinated water with six oxygen atoms located at 3.3 Å and a $\sigma^2 = 0.03$, corresponding to the approximate experimental value. The dashed line corresponds to the same geometry but with one of the water molecules replaced by a Rb^+ located at 3.41 Å at the expected contact ion pair distance. For Rb^+, an estimated $\sigma^2 = 0.03$ is used.

conclusion derived by D'Angelo et al.[31] in their study of the Br^-−water system under ambient conditions. The contribution to the XAFS from the second peak in the $G_{BrO}(R)$ is also a relatively minor component of the measured $\chi(k)$. The molecular configurations that were captured from the simulation were analyzed with FEFF using two different, maximum single scattering paths, 5 and 6 Å. The difference of these two spectra then contain only contributions from the 5−6 Å shell about the anion. This analysis showed that the contribution to $\chi(k)$ from the 5−6 Å shell is less than 4%. Again, this requires very high-resolution spectra in order to resolve this region.

There is evidence from molecular dynamics simulations of significant contact ion pairing occurring in fairly dilute supercritical salt solutions. It may be possible to use XAFS to detect ion pair formation, however, the observation of the contact ion pair is a poorly conditioned problem in this particular case because the Br^- to oxygen distance (3.3 Å) is very close to the estimated Br^- to Rb^+ distance (3.41 Å). Since the distances for the counter ion and the oxygen nearly coincide it is not possible to chemically identify adjoining Rb^+ ions with the *k* range of the data. This is confirmed in Figure 12 which shows FEFF-generated k^2-weighted $\chi(k)$ for two types of coordinated Br^-—one with an octahedrally coordinated water and the other with one water replaced by a Rb^+ ion at the expected contact ion pair distance. There are only subtle differences in the two spectra. Simulations by Chialvo et al.[6] suggest that under these supercritical conditions ion pairs (NaCl) are fully developed even at much lower concentrations than studied here. The presence of Rb^+ counter ions would lead to an error in the measured number of nearest neighbors *N*. From the FEFF simulation we estimate that this would lead to a measured *N* which is too large by about 15% due to the presence of the counter ion assuming that all of the Br^- anions are ion paired. The detection of contact ion pairs using XAFS is still possible using smaller ions where there is a larger percentage difference between the oxygen and the counter ion distances.

Conclusions

Results from both XAFS studies and MD simulation have been used to establish the dramatic changes in the hydration of bromide ion under supercritical conditions. The results have firmly established that extensive dehydration occurs under hydrothermal conditions. This is an unequivocal result that is not affected by the uncertainties of the other parameters. Inclusion of the anharmonicity parameter is required to obtain a correct measurement of the nearest-neighbor distances. There is qualitative agreement between the experimental results and the molecular dynamics simulation with respect to the number of nearest-neighbor waters, the nearest neighbor distances, the degree of disorder in the first shell and the trends of these parameters with increasing temperature. However, the results imply that the Br^-−water intermolecular potentials used in the MD simulations, which were parameterized under ambient conditions, must be substantially modified to quantitatively predict the behavior under supercritical conditions.

The effects of temperature, density, and solution concentration have been explored in detail. The primary factor affecting the decrease in hydration under supercritical conditions is the high temperature of the system. The fluid density and the salt concentration have only a minor effect on the hydration structure. These results have important implications for the transport, solubility and reactions of ionic species under supercritical conditions and, as such, provide us with a starting point for a much better understanding of a range of different effects in supercritical water systems.

Acknowledgment. This research was supported by the Director, Office of Energy Research, Office of Basic Energy Sciences, Chemical Sciences Division of the U.S. Department of Energy, under Contract DE-AC06-76RLO 1830. The authors would like to thank J. G. Darab of PNNL and D. K. Shuh and co-workers at LBNL for running standards at the SSRL. We thank L. Furenlid and F. Lu of beamline X19A at the National Synchrotron Light Source (operated by the U.S. Department of Energy) for their assistance.

Supporting Information Available: XAFS spectra for all conditions of the study, their corresponding background functions containing the multielectron excitation contribution (μ_0-(*E*)), and the Fourier transformed background functions, in addition to the k^2-weighted $\chi(k)$ plots and *R*-space plots for the data and the fits to the theoretical standard for all conditions (30 pages). Ordering information is given on any current masthead page.

References and Notes

(1) Thomason, T. B.; Modell, M. *Hazard. Waste* **1984**, *1*, 453.
(2) Shaw, R. W.; Brill, T. B.; Clifford, A. A.; Eckert, C. A.; Franck, E. U. *Chem. Eng. News* **1991**, *69*, 26−39.
(3) Balbuena, P. B.; Johnston, K. P.; Rossky, P. J. *J. Am. Chem. Soc.* **1994**, *116*, 2689−2690.
(4) Holgate, H. R.; Tester, J. W. *J. Phys. Chem.* **1994**, *98*, 800−809.
(5) Sealock, L. J.; Elliot, D. C.; Baker, E. G.; Butner, R. S. *Ind. Eng. Chem. Res.* **1993**, *32*, 1535−1541.
(6) Chialvo, A. A.; Cummings, P. T.; Cochran, H. D.; Simonson, J. M.; Mesmer, R. E. *J. Chem. Phys.* **1995**, *103*, 9379−9387.
(7) Oelkers, E. H.; Helgeson, H. C. *Science* **1993**, *261*, 888−891.

(8) Gao, J. *J. Phys. Chem.* **1994**, *98*, 6049−6053.
(9) Gorbaty, Y. E.; Kalinichev, A. G. *J. Phys. Chem*. **1995**, *99*, 5336−5340.
(10) Fernandez, D. P.; Mulev, Y.; Goodwin, A. R. H.; Sengers, J. M. H. *J. Phys. Chem. Ref. Data* **1995**, *24*, 33−69.
(11) Ding, K.; Seyfried, W. E. *Science* **1996**, *272*, 1634−1636.
(12) Pfund, D. M.; Darab, J. G.; Fulton, J. L.; Ma, Y. *J. Phys. Chem*. **1994**, *98*, 13102−13107.
(13) Palmer, B. J.; Pfund, D. M.; Fulton, J. L. *J. Phys. Chem*. **1996**, *100*, 13393−13398.
(14) Fulton, J. L.; Pfund, D. M.; Wallen, S. L.; Newville, M.; Stern, E. A.; Ma, Y. *J. Chem. Phys*. **1996**, *105*, 2161−2166.
(15) Yamaguchi, T.; Yamagami, M.; Ohzono, H.; Wakita, H.; Yamanaka, K. *Chem. Phys. Lett*. **1996**, *252*, 317−321.
(16) Seward, T. M.; Henderson, C. M. B.; Charnock, J. M.; Dobson, B. R. *Geochim. Cosmochim. Acta* 1996, *60*, 2273−2282.
(17) de Jong, P. H. K.; Neilson, G. W.; Bellissent-Funel, M. C. *J. Chem. Phys.* **1996**, *105*, 5155−5159.
(18) Sayers, D. E.; Stern, E. A.; Lytle, F. W. *Phys. Rev. Lett*. **1971**, *27*, 1204.
(19) Lee, P. A.; Citrin, P. H.; Eisenberger, P.; Kincaid, B. M. *Rev. Mod. Phys.* **1981**, *53*, 769−806.
(20) Lytle, F. W. In *Applications of Synchrotron Radiation*; Winick, H., Xian, D., Ye, M., Huang, T., Eds.; Gordon and Breach: New York, 1989; pp 135−223.
(21) Teo, B. K. *EXAFS: Basic Principles and Data Analysis*; Springer-Verlag: New York, 1986.
(22) Powell, D. H.; Neilson, G. W.; Enderby, J. E. *J. Phys.: Condens. Matter* **1993**, *5*, 5723−5730.
(23) Soper, A. K.; Neilson, G. W.; Enderby, J. E.; Howe, R. A. *J. Phys. C: Solid State Phys.* **1977**, *10*, 1793.
(24) Enderby, J. E. *Chem. Soc. Rev.* **1995**, 159−168.
(25) Cummings, S.; Enderby, J. E.; Neilson, G. W.; Newsome, J. R.; Howe, R. A.; Howells, W. S.; Soper, A. K. *Nature* **1980**, *287*, 714.
(26) Smith, D. E.; Dang, L. X. *Chem. Phys. Letters* **1994**, *230*, 209−214.
(27) Arshadi, M.; Yamdagni, R.; Kebarle, P. *J. Phys. Chem*. **1970**, *74*, 1475−1482.
(28) Hiraoka, K.; Mizuse, S.; Yamabe, S. *J. Phys. Chem*. **1988**, *92*, 3943−34952.
(29) Combariza, J. E.; Kestner, N. R.; Jortner, J. *J. Chem. Phys.* **1994**, *100*, 2851−2864.
(30) Xantheas, S. S.; Dunning, T. H. *J. Phys. Chem*. **1994**, *98*, 13489−13497.
(31) D'Angelo, P.; Di Nola, A.; Filipponi, A.; Pavel, N. V.; Roccatano, D. *J. Chem. Phys*. **1994**, *100*, 985−994.
(32) Sawa, Y.; Miyanaga, T.; Tanida, H.; Watanabe, I. *J. Chem. Soc., Faraday Trans*. **1995**, *91*, 4389−4393.
(33) Tanida, H.; Sakane, H.; Watanabe, I. *J. Chem. Soc., Dalton Trans*. **1994**, 2321−2326.
(34) Bertagnolli, H.; Ertel, T. S.; Hoffmann, M.; Fram, R. *Ber. Bunsen-Ges. Phys. Chem*. **1991**, *95*, 704−709.
(35) Ludwig, K. F.; Warburton, W. K.; Fontaine, A. *J. Chem. Phys.* **1987**, *87*, 620−629.
(36) Ohtaki, H.; Radnai, T. *Chem. Rev.* **1993**, *93*, 1157−1204.
(37) Stern, E. A.; Heald, S. In *Handbook of Synchrotron Radiation*; Eastman, D. E., Farge, Y., Koch, E. E., Eds.; North Holland: Amsterdam, 1983.
(38) Koningsberger, D. C., Prins, R., Eds. X-ray Absorption: Principles, Applications, Techniques of EXAFS, SEXAFS and XANES; John Wiley & Sons: New York, 1988.
(39) Newville, M.; Livins, P.; Yacoby, Y.; Rehr, J. J.; Stern, E. A. *Phys. Rev. B* **1993**, *47*, 14126−14131.
(40) Frenkel, A. I.; Stern, E. A.; Qian, M.; Newville, M. *Phys. Rev. B* **1993**, *48*, 12449−12458.
(41) Burattini, E.; D'Angelo, P.; Di Cicco, A.; Filipponi, A.; Pavel, N. V. *J. Phys. Chem*. **1993**, *97*, 5486−5494.
(42) D'Angelo, P.; Di Cicco, A.; Filipponi, A.; Pavel, N. V. *Phys. Rev. A* **1993**, *47*, 2055−2063.
(43) Tanida, H.; Sakane, H.; Watanabe, I.; Yokoyama, Y. *Chem. Lett.* **1993**, 1647−1650.
(44) Zabinsky, S. I.; Rehr, J. J.; Ankudinov, A.; Albers, R. C.; Eller, M. *J. Phys. Rev. B* **1995**, *52*, 2995−3009.
(45) Newville, M.; Ravel, R.; Haskel, D.; Rehr, J. J.; Stern, E. A.; Yacoby, Y. *Phys. B* **1995**, *208*,*209*, 154−156.
(46) Newville, M.; Stern, E. A. **1996**. In press.
(47) Abrahams, S. C.; Bernstein, J. L. *Acta Crystallogr*. **1977**, *B33*, 3601−3604.
(48) Lengeler, B. *Phys. Rev. Lett*. **1984**, *53*, 74−77.
(49) Dang, L. X. *J. Chem. Phys.* **1992**, *97*, 2659.
(50) Feller, D. F. Unpublished results.
(51) Dang, L. X. The parameters for bromine ion were supplied personally by Liem Dang. 1997.
(52) Bischoff, J. L.; Pitzer, K. S. *Am. J. Science* **1989**, *289*, 217−248.
(53) Chialvo, A. A.; Cummings, P. T. *J. Chem. Phys.* **1996**, *105*, 9248−9257.
(54) Balbuena, P. B.; Johnston, K. P.; Rossky, P. J. *J. Phys. Chem.* **1995**, *99*, 1554−1565.